

Arctic sea ice-free season projected to extend into fall

Marion Lebrun¹, Martin Vancoppenolle¹, Gurvan Madec¹, François Massonnet^{2,3}

¹ Sorbonne Université, LOCEAN-IPSL, CNRS/IRD/MNHN, Paris, France

² Earth and Life Institute, Université catholique de Louvain, Louvain-la-Neuve, Belgium

³ Earth Sciences Department, Barcelona Supercomputing Center, Barcelona, Spain

Revised manuscript submitted to *The Cryosphere*

Sep 5 2018

Marion Lebrun, Laboratoire d'Océanographie et du Climat, IPSL Boite 100, 4 Place Jussieu, 75252
Paris CEDEX 05, France.

22 **Abstract**

23

24 The recent Arctic sea-ice reduction is associated with an increase in the ice-free season
25 duration, with comparable contributions of earlier ice retreat and later advance. Here we show that
26 within the next decades, the trends towards later advance should progressively exceed and
27 ultimately double the trend towards an earlier ice retreat date, as robustly found in a hierarchy of
28 climate models. This comes from a strong feedback between earlier retreat and later advance, due to
29 a robust mechanism: the extra uptake of solar energy due to earlier retreat is absorbed about twice
30 as efficiently as heat is released in non-solar form before ice advance. By contrast, the winter
31 feedback of later advance onto earlier retreat is argued to be much weaker. Based on climate change
32 simulations, we envision an increase and a shift of the ice-free season towards fall, which will affect
33 Arctic ecosystems and navigation.

34 1. Introduction

35 Arctic sea ice has strikingly declined in coverage (Cavalieri and Parkinson, 2012), thickness
36 (Kwok and Rothrock, 2009; Renner et al., 2014; Lindsay and Schweiger, 2015) and age (Maslanik
37 et al., 2011) over the last four decades. CMIP5 global climate and Earth System Models simulate
38 and project this decline to continue over the 21st century (Massonnet et al., 2012; Stroeve et al.,
39 2012) due to anthropogenic CO₂ emissions (Notz and Stroeve, 2016), with a loss of multi-year ice
40 estimated for 2040-2060 (Massonnet et al., 2012), in the case of a business-as-usual emission
41 scenario.

42 Less Arctic sea ice also implies changes in ice seasonality, which are important to investigate
43 because of socio-economic (e.g., on shipping, Smith and Stephenson, 2013) and ecosystem
44 implications. Indeed, the length of the Arctic sea ice season exerts a first-order control on the light
45 reaching phytoplankton (Arrigo and van Dijken, 2011; Wassmann and Reigstad, 2011, Assmy et al.,
46 2017) and is crucial to some marine mammals, such as walruses (Laidre et al., 2015) and polar
47 bears (Stern and Laidre, 2016), who use sea ice as a living platform.

48 Various seasonality diagnostics are discussed in the sea ice literature and definitions as well
49 as approaches vary among authors. The open water season duration can be characterized from
50 satellite ice concentration fields, either as the number of ice-free days (Parkinson et al., 2014), or as
51 the time elapsed between ice retreat and advance dates, corresponding to the day of the year when
52 ice concentration exceeds or falls under a given threshold (Stammerjohn et al., 2012; Stroeve et al.,
53 2016). The different definitions of the length of the open water season can differ in subtleties of the
54 computations (notably filtering) and may not always entirely consistent and comparable. In
55 addition, the melt season duration, distinct from the open water season duration, has also been
56 analysed from changes in passive microwave emission signals due to the transition from a dry to a
57 wet surface during melting (Markus et al., 2009; Stroeve et al., 2014).

58 As for changes in the Arctic open water season duration, satellite-based studies indicate an
59 increase by >5 days per decade over 1979-2013 (Parkinson, 2014) due to earlier ice retreat and later
60 advance (Stammerjohn et al., 2012; Stroeve et al., 2016). There are regional deviations in the
61 contributions to a longer open water season duration, most remarkably in the Chukchi and Beaufort
62 Seas where later ice advance takes over (Johnson and Eicken, 2016; Serreze et al., 2016), which has
63 been attributed to increased oceanic heat advection from Bering Strait (Serreze et al., 2016). Such
64 changes in the seasonality of Arctic ice-covered waters reflect the response of the ocean surface
65 energy budget to warming. Indeed, warming and ice thinning imply earlier surface melt onset and
66 ice retreat (Markus et al., 2009; Stammerjohn et al., 2012; Blanchard-Wrigglesworth et al., 2010).
67 Besides, a shift towards later ice advance, tightly co-located with earlier retreat is observed,
68 especially where negative sea-ice trends are large (Stammerjohn et al., 2012; Stroeve et al., 2016).
69 This has been attributed to the ice-albedo feedback, namely to the combined action of (i) earlier ice
70 retreat, implying lower surface albedo and (ii) higher annual solar radiation uptake by the ocean.
71 Such mechanism (Stammerjohn et al., 2012) explains the ongoing delay in ice advance of a few
72 days per decade from the estimated increase in solar absorption (Perovich et al., 2007), in accord
73 the observed in situ increase in the annual SST maximum (Steele et al., 2008; Steele and Dickinson,
74 2016).

75 The observed increase in the ice-free season duration should continue over the next century,
76 as projected by the CESM-Large Ensemble (Barnhart et al., 2016), but this signal is characterized
77 by important levels of internal variability. Other CMIP5 ESMs likely project a longer ice season as
78 well, for sure in the Alaskan Arctic where they have been analysed (Wang and Overland, 2015). In
79 both these studies, the simulated future increases in the ice-free season duration are dominated by
80 the later ice advance. Such behaviour remains unexplained and should be investigated from a larger
81 set of models and regions.

82 In the present study, we aim at better quantifying the potential changes in Arctic sea ice
83 seasonality and understanding the associated mechanisms. We first revisit the ongoing changes in

84 Arctic sea ice retreat and advance dates using satellite passive microwave records, both at inter-
85 annual and multi-decadal time scales. We also analyse, for the first time over the entire Arctic, all
86 CMIP5 historical and RCP8.5 simulations covering 1900-2300 and study mechanisms at play using
87 a one-dimensional ice-ocean model.

88 **2. Methods**

89 We analyse the recent past and future of sea ice seasonality by computing a series of
90 diagnostics based on satellite observations, Earth System Models and a simple ice-ocean model.

91

92 **2.1 Data sources**

93 Passive microwave sea ice concentration (SIC) retrievals, namely the GSFC Bootstrap
94 SMMR-SSM/I quasi-daily time series product, over 1980-2015 (Comiso, 2000, updated 2015), are
95 used as an observational basis. We also use CMIP5 Earth System Model reconstructions and future
96 projections of SIC. Because of high inter-annual variability in ice advance and retreat dates and
97 because some models lose multi-year ice only late into the 21st century, we retain the 9 ESMs
98 simulations that pursue RCP8.5 until 2300 (first ensemble member, Table 1). Analysis focuses on
99 1900-2200, combining historical (1900-2005) and RCP8.5 (2005-2200) simulations. 2200
100 corresponds to the typical date of year-round Arctic sea ice disappearance (Hezel et al., 2014). We
101 also extracted the daily SST output from IPSL-CM5A-LR. All model outputs were interpolated on a
102 1° geographic grid.

103 Finally, to investigate how mean state biases may affect ESM simulations, we also included
104 in our analysis a 1958-2015 forced-atmosphere ISPL-CM simulation, i.e. an ice-ocean simulation
105 that was performed with the NEMO-LIM 3.6 model (Rousset et al., 2015), driven by the DFS5
106 atmospheric forcing (Dussin et al., 2015). NEMO-LIM 3.6 is very similar to the ice-ocean
107 component of IPSL-CM5A-LR, except that (i) horizontal resolution is twice as high (1° with
108 refinement near the poles and the equator) and (ii) a weak sea surface salinity restoring is applied.
109 Such a simulation, not only performs generally better than a free-atmosphere ESM run in terms of
110 seasonal ice extent (Fig S1; Uotila et al., 2017), but also has year-to-year variations in close
111 alignment with observations, a feature that is intrinsically beyond the capabilities of a free-
112 atmosphere ESM.

113 2.2 Ice seasonality diagnostics

114 We use slightly updated computation methods for ice retreat (d_r) and advance (d_a) dates, as
115 compared with previous contributions (Parkinson, 1994; Stammerjohn et al., 2012; and Stroeve et
116 al., 2016). Ice retreat date (d_r) is defined as the first day of the year where SIC drops below 15%,
117 whereas ice advance date (d_a) is the first day of the year where SIC exceeds this threshold (Stroeve
118 et al, 2016). Trends in d_r and d_a and cross-correlations have low sensitivity to the value of the SIC
119 threshold. All previous studies recognise that a typical 5-day temporal filtering on the input ice
120 concentration is required to get rid of short-term dynamical events (Stammerjohn et al., 2012;
121 Stroeve et al., 2016). By contrast, we use 15 days, in order to reduce noise due to short-term ice
122 events, which barely affects trends in d_r and d_a (see Table S1). Another important issue is the
123 reference time axis, which varies among authors. To circumvent the effect of the d_a discontinuity
124 between Dec 31 and Jan 1, we define the origin of time on Jan 1, and count d_a negatively if it falls
125 between Jul 1 and Dec 31. Jul 1 is a safe limit, because there is no instance of ice advance date
126 between early June and late July in the satellite record or in CMIP5 simulations. The length of the
127 ice-free season is defined as the period during which SIC is lower than 15%.

128 The same seasonality diagnostics are computed from model outputs. Yet, since the long-term
129 ESM simulations used here only have monthly SIC outputs, we compute the ice seasonality
130 diagnostics based on monthly SIC fields linearly interpolated daily. Such operation drastically
131 reduces error dispersion but introduces a small systematic bias on d_r (early bias) and d_a (late bias),
132 on the order of 5 ± 5 (6) days, which was determined from daily interpolation of monthly averaged
133 satellite data, see Fig S2. This small systematic bias in model ice retreat and advance dates likely
134 contributes to the mean model bias compared to satellite data (Table 1, Fig. 1), but remains small
135 compared to the long-term signals analysed throughout this paper.

136 The ice seasonality diagnostics and their spatial distribution are reasonably well captured by
137 the mean of selected CMIP5 models over the recent past (Fig. 2). Larger errors in some individual

models (Fig. S3) are associated with an inaccurate position of the ice edge. Overall, ESMs tend to have a shorter open water season than observed (Fig 2a-c and S3), which is tangible in the North Atlantic and North Pacific regions and can be related to the systematic bias due to the use of interpolated monthly data, but also to the tendency of our model subset to overestimate sea ice. Such an interpretation is supported by (i) the visibly better consistency of the simulated ice seasonality diagnostics with observations in the forced-atmosphere ISPL-CM simulation than in IPSL-CM5A-LR and (ii) by the fact that models with simulated ice extent rather close to observations over the recent past (CESM, CNRM or MPI; Massonnet et al., 2013) are more in line with observed seasonality diagnostics than the other models (Fig. 2 and S3).

2.3. Trends in ice advance and retreat dates, and related diagnostics

Trends in ice retreat and advance dates were calculated for each satellite or model pixel, from the slope of a least-square fit over a given period, using years where both d_r and d_a are defined. If the number of years used for calculation of the trend is less than 1/3 of the considered period, a missing value is assigned. 1/3 compromises between spatial and temporal coverage of the considered time-series (see Tab. S1).

To describe the relative contribution of ice advance and retreat dates to changes in open water season duration, we introduce a first diagnostic, termed the *long-term ice advance vs. retreat amplification coefficient* ($R_{a/r}^{long}$). $R_{a/r}^{long}$ is defined as minus the ratio of trends in ice advance to trends in ice retreat dates. The sign choice for $R_{a/r}^{long}$ is such that positive values arise for concomitant long-term trends toward later ice advance and earlier retreat. $R_{a/r}^{long}$ gives synthetic information about trends in ice advance and retreat dates within a single diagnostic. For example, $R_{a/r}^{long} > 0$ means that a trend towards earlier retreat ($d_r < 0$) corresponds a trend towards later advance ($d_a > 0$). Moreover, by definition, $R_{a/r}^{long} > 1$ if the long-term trend in ice advance date exceeds the long-term trend in retreat date in a particular pixel, otherwise $R_{a/r}^{long} < 1$. Note that for

162 $R_{a/r}^{long}$ to be meaningful, we restrict computations to pixels where trends in both d_r and d_a are
163 significant at a specified confidence level. $p=0.05$, i.e a 95% confidence interval gives the most
164 robust value but heavily restricts the spatial coverage, especially for CMIP5 outputs. By contrast,
165 $p=0.25$, i.e. a 75% confidence interval slightly expands coverage, but loses some robustness.

166 In order to study the shorter-term association between retreat and ice advance, we introduce a
167 second diagnostic, termed the *short-term ice advance vs retreat amplification coefficient* ($R_{a/r}^{short}$).
168 $R_{a/r}^{short}$ is defined by applying the same reasoning to inter-annual time scales, as minus the linear
169 regression coefficient between detrended ice advance and retreat dates. $R_{a/r}^{short}$ gives information on
170 how anomalies in ice advance date scale with respect to anomalies in retreat dates over the same
171 year, regardless of the long-term trend. Such definition warrants comparable interpretation for
172 $R_{a/r}^{short}$ and $R_{a/r}^{long}$. $R_{a/r}^{short} > 0$ indicates concomitant anomalies towards earlier retreat and later
173 advance, and $R_{a/r}^{short} > 1$ indicates that anomalies in advance date are larger than in retreat date.

174 For computations of $R_{a/r}^{long}$ and $R_{a/r}^{short}$ we use reference periods of either 36 or 200 years. 36
175 years is the length of the available observation period and is close to the standard 30 years used in
176 climate sciences. 200 years is the total amount of years we can use to qualify changes and the most
177 representative of a long climate change simulation.

178 All trends and ice advance vs. retreat amplification coefficients given in the rest of the text are
179 median (\pm inter-quartile range), taken over the seasonal ice zone. We use non-parametric statistics
180 because the distributions are not Gaussian.

181

182 **2.4 1D model**

183 We use the Semtner (1976) zero-layer approach for ice growth and melt above an upper
184 oceanic layer taking up heat, whereas snow is neglected. The model simplifies reality by assuming
185 constant mixed-layer depth, no horizontal advection in ice and ocean, and no heat exchange with
186 the interior ocean. The ice-ocean seasonal energetic cycle is computed over 300 years, using

187 climatological solar, latent and sensible heat fluxes and increasing downwelling long-wave
188 radiation, to represent the greenhouse effect. Ice retreat and advance dates are diagnosed from
189 model outputs (see Appendix A for details).

190

191 3. Link between earlier ice retreat and later ice advance in observations and models

192 3.1 Trends in ice advance and retreat date in observations and models

193 Over 1980-2015, the ice-free season duration has increased by 9.9 ± 10.6 days / decade, with
194 nearly equal contributions of earlier ice retreat (-4.8 ± 7.7 days / decade) and later ice advance (4.9
195 ± 5.8 days /decade, median based on satellite observation, updated figures, see Table S1).
196 Variability is high however, and trends are generally not significant, except over a relatively small
197 fraction (22%) of the seasonal ice zone (Fig. 3), independently of the details of the computation
198 (Tab. S1). The patterns of changes are regionally contrasted, and Chukchi Sea is the most notable
199 exception to the rule, where later ice advance clearly dominates changes in the ice-free season
200 (Serreze et al., 2016, Fig. 3).

201 Simulated trends by the mean of selected CMIP5 models are comparable with observations, in
202 terms of ice retreat date (-4.4 ± 3.5 days / decade), ice advance date (5.9 ± 3.3 days / decade) and
203 ice-free season duration (10.3 ± 6.3 days / decade) (Fig. 3). Individual models show larger errors
204 (Fig. S4 to compare with Fig.3), to be related notably with mean state issues. One common location
205 where trends are underestimated is the North Atlantic region, in particular Barents Sea, which
206 arguably reflects a weak meridional oceanic heat supply (Serreze et al.,2016).

207

208 3.2 Earlier sea ice retreat implies later ice advance

209 In terms of mean state and contemporary trends, models seem realistic enough for an analysis
210 of changes at pan-Arctic scales but might be less meaningful at regional scales. We first study the
211 contemporary link between earlier retreat and ice advance by looking at the sign of $R_{a/r}$'s in
212 contemporary observations and models. Because $R_{a/r}^{long}$ is a ratio of significant trends, and because
213 all models have regional differences as to where trends are significant, we base our analysis on
214 individual models.

215 Based on observations (Fig. 4), we find positive values of $R_{a/r}^{long}$ in more than 99% of grid
 216 points in the studied zone, provided that computations are restricted where trends on ice retreat and
 217 advance dates are significant at a 95% level (N=5257). Positive $R_{a/r}^{long}$ values mean concomitant and
 218 significant trends towards both earlier retreat and advance, whereas missing values reflect either
 219 that the trends are not significant or that the point is out of the seasonal ice zone. $R_{a/r}^{short}$ (Fig. 5) is
 220 generally smaller (0.21 ± 0.27) than $R_{a/r}^{long}$ (0.71 ± 0.42 , 95% confidence level), and also positive in
 221 most pixels (87% of 23475 pixels).

222 CMIP5 models are thus consistent with the robust link between earlier ice retreat and later
 223 advance dates found in observations (Stammerjohn et al., 2012; Stroeve et al., 2016). More
 224 generally, we find a robust link between earlier retreat and later advance in all cases: both $R_{a/r}$'s are
 225 virtually always positive for short and long-term computations, from observations and models (Fig.
 226 4, 5) over the three analysed periods (1980-2015 for observations and models, 2015-2050 and 2050-
 227 2085 for models only) and regardless of internal variability (Fig S5 and S6). This finding expands
 228 previous findings from satellite observations using detrended time series (Stammerjohn et al., 2012;
 229 Serreze et al, 2016; Stern and Laidre, 2016), in particular the clear linear correlation found between
 230 detrended ice retreat and ice advance dates (Stroeve et al., 2016). Following these authors, we
 231 attribute the strong earlier retreat / later ice advance relationship as a manifestation of the ice-albedo
 232 feedback: earlier ice retreat leads to an extra absorption of heat by the upper ocean. This heat must
 233 be released back to the atmosphere before the ice can start freezing again, leading to later ice
 234 advance. This explanation is also supported by satellite SST analysis in the ice-free season (Steele et
 235 al., 2008; Steele and Dickinson, 2016).

236

237 3.3 Increasingly late ice advance dominates future changes in open water season

238 We now focus on the respective contribution of changes in retreat and ice advance dates to the
239 increasingly long open water season, by analysing the magnitude of $R_{a/r}^{long}$. Contemporary values of
240 $R_{a/r}^{long}$ match between model and observations but not spatially (Fig. 4). Over 1980-2015 the
241 simulated $R_{a/r}^{long}$ (CMIP5 mean) is slightly higher (1.1 ± 0.7) than the observational value ($0.7 \pm$
242 0.4). Since none of the models positions the sea ice edge correctly everywhere, it is not surprising
243 that the spatial distribution and the modal $R_{a/r}^{long}$ differs among models and between models and
244 observations. Indeed, the forced-atmosphere ISPL-CM simulation better simulates the spatial
245 distribution of $R_{a/r}^{long}$ (see Fig. S7), which underlines the role of mean state errors.

246 As far as future changes are concerned, all models show a qualitatively similar evolution (Fig.
247 1 and S5). Projected changes in ice retreat and ice advance dates start by approximately 2000 and
248 continue at a nearly constant pace from 2040 until 2200. By 2040, the trend in ice advance date
249 typically becomes larger than the trend in ice retreat date, as indicated by the corresponding mean
250 $R_{a/r}^{long} = 1.8 \pm 0.4$ over 2000-2200 (Table 1).

251 To further understand these contrasting trends between ice retreat and ice advance dates, we
252 mapped $R_{a/r}^{long}$, over 2015-2050 and 2050-2085. We find that, in the course of the 21st century,
253 trends in retreat and ice advance date become significant over increasingly wide regions. The
254 overall $R_{a/r}^{long}$ value increases, as illustrated in Fig. 4. This behaviour is found independent of the
255 considered model and of the internal variability (Fig. S5 and S6).

256 This finding expands the recent analyses of the CESM Large-Ensemble project (Barnhart et
257 al., 2016); and of Alaskan Arctic sea ice in CMIP5 models, finding faster ice coverage decrease in
258 fall than in spring (Wang and Overland, 2015). Both studies propose that the extra heat uptake in
259 the surface ocean due to an increased open water season as a potential explanation. As suggested

earlier, this indeed explains why $R_{a/r}^{long}$ would be positive but does not explain the amplified delay in ice advance date, or why $R_{a/r}^{long}$ would be > 1 .

3.4 A thermodynamic mechanism for an amplified delay in ice advance date

The reason why $R_{a/r}^{long}$ becomes > 1 by 2040 is related to the asymmetric response of ice-ocean thermodynamics to warming. Such response emerges from simulations with a 1D thermodynamic model of sea ice growth and melt in relation with the upper ocean energy budget (Semtner, 1976). Without any particular tuning, the 1D model simulations feature an evolution that is similar to the long-term behaviour of CMIP5 models (Fig. 1b), with trends in ice advance date (6.0 days/decade) of larger absolute magnitude than trends in retreat date (-3.1 days/decade), with a corresponding value of $R_{a/r}^{long} = 1.9$, all numbers falling within the CMIP5 envelope (Tab. 1).

The ultimate driver of the changes in ice seasonality is the applied radiative forcing. A 0.1 W/m² increase has a direct impact of about 0.5 d/yr of both earlier retreat and later advance. Because of non-linearities in the system, there are also two feedbacks between ice advance and ice retreat dates. The contribution of later advance to earlier retreat at the end of the subsequent melt season is of ~25% and constitutes a relatively weak amplifying winter feedback. Why it is the case is first because ice has generally more time to grow than it has to melt (Perovich et al., 2003). Hence, provided that the growth and melt do not change too much, changes in ice advance translate into weaker changes in ice retreat date. The second reason is the inverse dependence of ice growth rates to thickness which implies that thin ice grows faster than thick ice (Maykut, 1986). Because of this, the maximum winter ice thickness does not decrease due to later advance as much as if the growth rate was constant.

The summer feedback also contributes to amplify changes and is comparatively much stronger: the contribution of earlier retreat to changes towards later ice advance is between 100 and 200%. The strength of this feedback is in direct relation with the upper ocean energy budget and the

285 evolution of SST, in a way that goes beyond the classical ice-albedo feedback explanation. After ice
 286 retreat, the SST rapidly increases due to solar absorption into the mixed layer and then decreases
 287 much slower until freezing, due to non-solar ocean-to-atmosphere fluxes (Fig. 6a), an evolution that
 288 is similar to a recent satellite-based analysis (Steele and Dickinson, 2016).

289 The 1D model framework provides means to diagnose this mechanism. The energy excess
 290 associated with later retreat stored into the surface ocean takes extra time to be released before ice
 291 advance. Hence, from energy conservation, a simple expression linking $R_{a/r}^{long}$ (the seasonality of the
 292 system) and ice-free ocean heat fluxes can be derived (see Appendix A):

$$293 \quad R_{a/r}^{long} \cong Q_+/Q_-,$$

294 where Q_+ and Q_- are the absolute values of average net positive (negative) atmosphere-to-ocean
 295 heat fluxes during the ice free-period. Q_+ mostly corresponds to net solar flux, typically 150 W/m²,
 296 whereas Q_- corresponds to the net non-solar, mostly long-wave heat flux, at freezing temperatures,
 297 typically 75-150 W/m² (See Appendix B). Since $Q_+ \geq Q_-$, $R_{a/r}^{long} \geq 1$ and hence the delay in ice
 298 advance date is larger than the delay in retreat date.

299 Why $R_{a/r}^{long}$ would vary so little among CMIP5 models and even the 1D model is because
 300 celestial mechanics, ubiquitous clouds and near-freezing temperatures provide strong constraints on
 301 the surface radiation balance, that all models likely capture. All models also include the growth and
 302 melt season asymmetry and the growth-thickness relationship at the source of the relatively weak
 303 winter feedback. In IPSL-CM5A-LR, the sole model for which we could retrieve daily SST (Fig.
 304 6b), the evolution of the summer SST in seasonally ice-free regions features a rapid initial increase
 305 followed by slow decrease, an indication that the mechanism we propose is sensible.

306

307 **3.5 Inter-annual variability and extra processes add to the purely thermodynamic response**

308 $R_{a/r}^{long} > 1$ only clearly emerges by 2040 in CMIP5 models, whereas $R_{a/r}^{long}$ is typically < 1 over
 309 the recent past (1980-2015) from the satellite record (Fig. 4). There are physical arguments in
 310 favour of a progressive emergence of a 1D response in the course of this century. (i) The
 311 contribution of the sub-surface ocean to the surface energy budget, neglected in the 1D approach, is
 312 likely larger today than in the future Arctic. Over the 21st century, the Arctic stratification increases
 313 in CMIP5 models (Vancoppenolle et al., 2013; Steiner et al., 2014), whereas the oceanic heat flux
 314 convergence should decrease (Bitz et al., 2005). (ii) It seems also clear that the solar contribution to
 315 the upper ocean energy budget is smaller today than in the future, as the date of retreat falls closer
 316 to the summer solstice. (iii) The surface energy budget is less spatially coherent today than in the
 317 future, when the seasonal ice zone moves northwards. The solar radiation maximum drastically
 318 changes over 45 to 65°N but has small spatial variations above the Arctic circle (Peixoto and Oort,
 319 1992). In some specific regions, $R_{a/r}^{long}$ is already > 1 , in particular in Chukchi Sea, but this has been
 320 associated to the summer oceanic heat transport through Bering Strait (Serreze et al., 2016) which is
 321 a localized event, that does not explain why $R_{a/r}^{long}$ would globally become > 1 in the future. The
 322 aforementioned processes, ignored in the 1-D model may explain why $R_{a/r}^{long} > 1$ would emerge by
 323 mid-century, but inter-annual variability, also absent in the 1-D model, should also be considered
 324 (Barnhart et al., 2016). It is remarkable that $R_{a/r}^{short}$ is < 1 both from satellite records and from
 325 CMIP5 model simulations, for all periods and models considered (Fig. 5). This suggests that the ice
 326 advance amplification mechanism is not dominant at inter-annual time scales. Indeed, based on
 327 inter-annual satellite time series, the standard deviation of ice retreat (STD=21.6 days) and advance
 328 dates (STD=14.3 days) is high (Stroeve et al., 2016) and the corresponding trends over 1980-2015
 329 are not significant. Conceivably, atmosphere, ocean and ice horizontal transport, operating at
 330 synoptic to inter-annual time scales, obscure the simple thermodynamic relation between the ice
 331 retreat and advance dates found in the 1D model. Altogether, this highlights that the ice advance
 332 amplification mechanism is a long-term process and stress the importance of the considered time

333 scales and period as previous studies have already shown (Parkinson et al., 2014; Barnhart et al.,
334 2016).

335

336 4. Conclusions

337 The present analysis, focused on contemporary and future changes in sea ice seasonality,
338 based on satellite retrievals and Earth System Model simulations of ice coverage, raised the
339 following key findings:

340 1. The 1980-2015 long-term trends in ice retreat and advance dates are of similar
341 magnitude but still insignificant over 78% of the seasonal ice zone.

342 2. CMIP5 models consistently project a long-term rate of change in ice advance date
343 that is about twice as large as the rate of change in ice retreat date: the open water season shifts
344 into fall.

345 3. The reduced surface albedo and the enhanced solar radiation uptake by the ocean had
346 previously been put forward to explain such changes in sea ice seasonality. Next to these two
347 elements, our analysis highlights a third, new element: the comparatively slow heat loss by ice-
348 free waters before ice advance, which is the key contributor to the amplified delay in ice advance
349 date.

350 More generally, thermodynamic processes exert a central control on sea ice seasonality. The
351 ice-albedo feedback provides a strong link between earlier ice retreat and later advance, a link that
352 is found in both satellite retrievals and climate projections, regardless of the considered period and
353 time scale, expanding findings from previous works (Stammerjohn et al., 2012; Serreze et al, 2016;
354 Stern and Laidre, 2016; Stroeve et al., 2016). Why long-term trends in ice advance date are
355 ultimately about twice as large as the trends in ice retreat date is also of thermodynamic origin:
356 extra solar heat reaching the ocean due to earlier ice retreat is absorbed at a higher rate than it can
357 be released until ice advance. The long-term response to warming of ice seasonality turns up by
358 mid-century in CMIP5 simulations, when changes in the ice-free season emerge out of variability
359 (Barnhart et al., 2016).

360 The absence of an ice advance amplification at inter-annual time scales is in contradiction
361 with the thermodynamic response of seasonal ice to warming. This points to dynamical processes as
362 most likely drivers, a setup that would have other analogs in climate change studies (Bony et al.,
363 2004; Kröner et al., 2017; Shepherd, 2014), but would need further analysis for confirmation. The
364 suggested increase in the ice-free season and shift into fall are part of broader seasonal changes in
365 the climate system. Global warming induces changes in the seasonal cycle of surface temperature
366 (Thomson, 1995), both in terms of amplitude and phase (Dwyer et al., 2012), in relation with the
367 surface energy fluxes and the presence of sea ice (Dwyer et al., 2012; Donohoe and Battisti, 2013).

368 As the Arctic sea ice seasonality is a basic trait of the Arctic Ocean, a shift of the Arctic sea
369 ice-free season would also have direct ecosystem and socio-economic impacts. The shift in the sea
370 ice seasonal cycle will progressively break the close association between the ice-free season and the
371 seasonal photoperiod in Arctic waters, a relation that is fundamental to photosynthetic marine
372 organisms existing in present climate (Arrigo and van Dijken, 2011). Indeed, because the ice
373 advance date is projected to overtake the onset of polar night (Fig. 1), typically by 2050, changes in
374 the photoperiod are at this point solely determined by the ice retreat date, and no more by advance
375 date. The duration of the sea ice season also affects travel and hunting habits of coastal human
376 communities (Huntington et al, 2017) and restricts the shipping season (Smith and Stephenson,
377 2013; Melia et al., 2017). The second clear implication of the foreseen shift of the Arctic open
378 water season is that the Arctic navigability would expand to fall, well beyond the onset of polar
379 night, supporting the lengthening of the shipping season mostly by later closing dates (Melia et al.,
380 2017).

381 Better projecting future changes in sea ice and its seasonality is fundamental to our
382 understanding of the future Arctic Ocean. Detailed studies of the drivers of sea ice seasonality, in
383 particular the upper ocean energy budget, the role of winter and summer feedbacks and the
384 respective contribution of thermodynamic and dynamic processes are possible tracks towards
385 reduced uncertainties. Further knowledge can be acquired from observations (e.g. Steele and

386 Dickinson, 2016) and Earth System Model analyses, for which the expanded set of ice-ocean
387 diagnostics expected in CMIP6, including daily ice concentration fields (Notz et al., 2016) will
388 prove instrumental.

389 **Code, data and sample availability**

390 Scripts available upon request.

391 Contact: Marion Lebrun, Laboratoire d'Océanographie et du Climat, IPSL Boite 100, 4 Place

392 Jussieu, 75252 Paris CEDEX 05, France.

393 Appendices

394 Appendix A: Upper ocean energetics and ice seasonality in the 1D ice-ocean model

395 We use the Semtner (1976) zero-layer approach for ice growth and melt above an upper oceanic
396 layer taking up heat. Snow is neglected. The ice model equations for surface temperature (T_{su}) and
397 ice thickness (h) read:

$$398 \quad Q_{atm}(T_{su}) = Q_c(T_{su}), \quad (1)$$

$$399 \quad \rho L \frac{dh}{dt} = Q_{atm}(T_{su}) + Q_w. \quad (2)$$

400 where $Q_{atm} = Q_0 + Q_{sol}(1 - \alpha_i) - \epsilon\sigma T_{su}^4$, with Q_0 the sum of downwelling longwave, latent and
401 sensible heat fluxes, Q_{sol} the incoming solar flux, $\alpha_i = 0.64$ the ice albedo, $\epsilon = 0.98$ the emissivity
402 and $\sigma = 5.67 \times 10^{-8} W/m^2/K^4$ the Stefan-Boltzmann constant. Q_c is the heat conduction flux in
403 the ice (> 0 downwards), Q_w is the ocean-to-ice sensible heat flux at the ice base, $\rho = 900 kg/m^3$
404 is ice density and $L = 334 kJ/kg$ is the latent heat of fusion. Once the ice thickness vanishes, the
405 water temperature T_w in a $h_w = 30m$ -thick upper ocean layer follows:

$$406 \quad \rho_w c_w \frac{\partial T_w}{\partial t} h_w = Q_0 + Q_{sol}(1 - \alpha_w)[1 - \exp(-\kappa h_w)] - \epsilon\sigma T_w^4. \quad (3)$$

407 $\rho_w = 1025 kg/m^3$ is water density, $c_w = 4000 J/kg/K$ is water specific heat, $\kappa_w = 1/30 m^{-1}$ is
408 the solar radiation attenuation coefficient in water. Ice starts forming back once T_w returns to the
409 freezing point $T_f = -1.8^\circ C$.

410 The atmospheric solar (Q_{sol}) and non-solar (Q_0) heat fluxes are forced using the classical standard
411 monthly mean climatologies, typical of Central Arctic conditions (Fletcher, 1965). We add an extra
412 $Q_{nsol} = 0.1 W/m^2$ to the non-solar flux each year to simulate the greenhouse effect. We impose
413 $Q_w = 2 W/m^2$ following Maykut and Untersteiner (1971). Ice becomes seasonal after 127 years.
414 The model is run until there is no ice left, which takes 324 years.

415 The following three diagnostics are used to describe the ice-ocean seasonality (see Fig. 1):

416 • d_r (*ice retreat date*): the first day with $T_w > T_f = -1.8^\circ\text{C}$;

417 • d_a (*ice advance date*): the last day with $T_w > T_f = -1.8^\circ\text{C}$;

418 • d_{max} (*maximum water temperature date*): the last day with $Q > 0$.

419 Let us now detail how the ratio of ice advance and retreat dates trends, R_a^{long} , is related to the

420 energy budget of the ice-free ocean in the 1-D model. We first express the relation between ice

421 advance and retreat dates for a given year. Since heat fluxes are strongly constrained by the

422 imposed forcing, the ice advance date d_a is directly connected with d_r . Once ice has disappeared

423 on $d = d_r$, the upper ocean takes up energy and warms from the freezing point until T_w is

424 maximum on $d = d_{max}$. Then the upper ocean loses energy until T_w returns to the freezing point

425 ($d = d_a$). Over this temperature path, the energy gain from d_a to d_{max} must equal the energy loss

426 from d_{max} to d_a , which can be written as:

427
$$Q_+(d_{max} - d_r) = -Q_-(d_a - d_{max}), \quad (4)$$

428 where $Q_+(> 0)$ is defined as the average net heat flux to the upper ocean over $[d_r, d_{max}]$ and $Q_-(<$

429 $0)$ is the average net heat flux over $[d_{max}, d_a]$. Referring d_r and d_f with respect to d_{max} :

430
$$d'_r = d_r - d_{max}, \quad (5)$$

431
$$d'_a = d_a - d_{max}, \quad (6)$$

432 and defining the ice-free ocean energetic ratio as $R_Q \equiv Q_+/Q_-$, Eq. (4) simplifies into:

433
$$d'_a = R_Q d'_r. \quad (7)$$

434 In other words, the time difference between ice advance date and upper ocean temperature

435 maximum is R_Q times the difference between the dates of maximum water temperature and ice

436 retreat. In practice, Q_+ is always higher than Q_- , hence R_Q is always >1 , i.e., the heat enters into the

437 upper ocean faster than it escapes, T_w increases faster than it decreases and $d'_a > d'_r$. Note that the

438 relation (7) is not valid in reality because of ice dynamics and other three-dimensional processes.

439 We now seek to express the change in ice advance date Δd_a as a function of the change in ice
 440 retreat date Δd_r , over two different years (labelled with subscripts 1 and 2), because of a change in
 441 atmospheric forcing. Using d_{max} as the origin of time, Δd_r and Δd_a can be expressed as:

$$442 \quad \Delta d_r = d'_{r,2} - d'_{r,1} - \Delta d_{max}, \quad (8)$$

$$443 \quad \Delta d_a = d'_{a,2} - d'_{a,1} - \Delta d_{max}. \quad (9)$$

444 Multiplying Eq. (8) by $R_{Q,2}$, then using Eq. (7) in Eq. (8) to substitute $d'_{r,1} = d'_{a,1}/R_{Q,1}$ and in Eq.
 445 (9) to substitute $d'_{a,2} = R_{Q,2}d'_{r,2}$, then subtracting Eq. (9) from Eq. (8), and finally rearranging
 446 terms, one retrieves the shift in ice advance date:

$$447 \quad \Delta d_a = R_{Q,2}\Delta d_r + \left(\frac{R_{Q,2}}{R_{Q,1}} - 1\right)d'_{a,1} + (1 - R_{Q,2})\Delta d_{max}, \quad (10)$$

448 which is an exact solution (see Fig. A1). A good approximation to this can be found by assuming
 449 that years 1 and 2 are not too far in time, $R_2 \approx R_1$ and $\Delta d_{max} \approx 0$, hence the last two terms drop
 450 and the shift in ice advance date further simplifies into:

$$451 \quad \Delta d_a \approx R_{Q,2}\Delta d_r = \frac{Q_{+,2}}{Q_{-,2}}\Delta d_r. \quad (11)$$

452 The shift in ice advance date is thus nearly equal to the shift in ice retreat date multiplied by the $\frac{Q_+}{Q_-}$
 453 ratio and is therefore always higher than Δd_r . This last equation provides a concise and powerful
 454 simplification of the energetics of the system under consideration. It states that, in the Semtner
 455 (1976) zero-layer one-dimensional idealised ice-ocean system, the response of the seasonality of the
 456 ice cover to changes in atmospheric forcing can be directly estimated from the surface energy
 457 balance of the ice-free ocean.

458

459 **Appendix B: scaling of the ice-free ocean energy budget**

460 1D model results show a direct link between, on the one hand, the ratio of long-term trends in ice
 461 advance and retreat date ($R_{a/r}^{long}$), and the energetics of the ice-free ocean on the other hand:

$$462 \quad R_{a/r}^{long} = Q_+/Q_-,$$

463 where Q_+ and Q_- are the absolute values of average net positive (negative) atmosphere-to-ocean
 464 heat fluxes during the ice free-period. CMIP6 and 1D model results suggest that over long-time
 465 scales, this ratio is stable and does not vary much among models, with values ranging from 1.5 to 2.
 466 Why this ratio would be so invariable is because celestial mechanics, ubiquitous clouds and near-
 467 freezing temperatures provide strong constraints on the radiation balance, which dominates the
 468 surface energy budget.

469 Assuming that non-solar components cancel each other, the mean heat gain is mostly solar:

$$470 \quad Q_+ = \langle Q_{sol}(1 - \alpha_w)[1 - \exp(-\kappa h_w)] \rangle |_{early\ ice-free\ season},$$

471 where the mean is taken over the first part of the ice-free period, typically covering July or June. Of
 472 remarkable importance is that the magnitude of clear-sky solar flux above the Arctic Circle deviates
 473 by less than 20 W/m², both in space and time, around the summer solstice (see, e.g., Peixoto and
 474 Oort, 1992). Assuming summer cloud skies would remain the norm, we take 150 W/m² as
 475 representative for Q_+ .

476 The mean heat loss is mostly non-solar:

$$477 \quad Q_- = -\langle Q_{lw} - \epsilon\sigma T_w^4 + Q_{sh} + Q_{lh} \rangle |_{late\ ice-free\ season},$$

478 and corresponds to the second part of the ice-free period, typically covering September and
 479 October. Downwelling long-wave radiation flux Q_{lw} corresponds to cloud skies at near freezing
 480 temperatures, for which 250 W/m² seems reasonable (Persson et al., 2002). The thermal emission
 481 would be that of the ocean, a nearly ideal black body, at near-freezing temperatures, and should not
 482 depart much from 300 W/m². The sensible (Q_{sh}) and latent (Q_{lh}) heat fluxes are relatively more

483 uncertain. In current ice-covered conditions, turbulent fluxes imply a net average heat loss, typically
484 smaller than 10 W/m^2 (Personn et al., 2002). Over an ice-free ocean however, turbulent heat losses
485 would obviously increase, in particular through the latent heat flux, but also become more variable
486 at synoptic time scales. Assuming that turbulent heat fluxes would in the future Arctic compare to
487 what they are today in ice-free ocean regions of the North Pacific, we argue that they would
488 correspond to a 25 W/m^2 heat loss, definitely not exceeding 100 W/m^2 (Yu et al., 2008).

489 Taken together, these elements give an estimated R value ranging from 1 to 2, where uncertainties
490 on the dominant radiation terms of the energy budget are small and inter-model differences in
491 turbulent heat fluxes would be decisive in determining the actual value of the ratio.

492

493 **Author Contribution**

494 All authors conceived the study and co-wrote the paper. ML and MV performed analyses.

495

496 **Competing contribution**

497 The authors declare that they have no conflict of interest.

498

499 **Acknowledgements**

500 We thank Sebastien Denvil for technical support; and Roland Seferian, Jean-Baptiste Sallée, Olivier

501 Aumont and Laurent Bopp for scientific discussions. We also thank the anonymous reviewers for

502 their constructive comments that helped to improve the paper.

503 **References**

- 504 Arrigo, K. R. and van Dijken, G. L.: Secular trends in Arctic Ocean net primary production, J.
505 Geophys. Res., 116(C9), C09011, doi:[10.1029/2011JC007151](https://doi.org/10.1029/2011JC007151), 2011.
- 506 Assmy, P., Fernández-Méndez, M., Duarte, P., Meyer, A., Randelhoff, A., Mundy, C. J., Olsen, L.
507 M., Kauko, H. M., Bailey, A., Chierici, M., Cohen, L., Doulgeris, A. P., Ehn, J. K., Fransson, A.,
508 Gerland, S., Hop, H., Hudson, S. R., Hughes, N., Itkin, P., Johnsen, G., King, J. A., Koch, B. P.,
509 Koenig, Z., Kwasniewski, S., Laney, S. R., Nicolaus, M., Pavlov, A. K., Polashenski, C. M.,
510 Provost, C., Rösel, A., Sandbu, M., Spreen, G., Smedsrud, L. H., Sundfjord, A., Taskjelle, T.,
511 Tatarek, A., Wiktor, J., Wagner, P. M., Wold, A., Steen, H. and Granskog, M. A.: Leads in Arctic
512 pack ice enable early phytoplankton blooms below snow-covered sea ice, Scientific Reports, 7,
513 srep40850, doi:[10.1038/srep40850](https://doi.org/10.1038/srep40850), 2017.
- 514 Barnhart, K. R., Miller, C. R., Overeem, I. and Kay, J. E.: Mapping the future expansion of Arctic
515 open water, Nature Clim. Change, 6(3), 280–285, doi:[10.1038/nclimate2848](https://doi.org/10.1038/nclimate2848), 2016.
- 516 Bitz, C. M., Holland, M. M., Hunke, E. C. and Moritz, R. E.: Maintenance of the Sea-Ice Edge, J.
517 Climate, 18(15), 2903–2921, doi:[10.1175/JCLI3428.1](https://doi.org/10.1175/JCLI3428.1), 2005.
- 518 Blanchard-Wrigglesworth, E., Armour, K. C., Bitz, C. M. and DeWeaver, E.: Persistence and
519 Inherent Predictability of Arctic Sea Ice in a GCM Ensemble and Observations, J. Climate, 24(1),
520 231–250, doi:[10.1175/2010JCLI3775.1](https://doi.org/10.1175/2010JCLI3775.1), 2010.
- 521 Bony, S., Dufresne, J.-L., Treut, H. L., Morcrette, J.-J. and Senior, C.: On dynamic and
522 thermodynamic components of cloud changes, Climate Dynamics, 22(2–3), 71–86,
523 doi:[10.1007/s00382-003-0369-6](https://doi.org/10.1007/s00382-003-0369-6), 2004.
- 524 Cavalieri, D. J. and Parkinson, C. L.: Arctic sea ice variability and trends, 1979–2010, The
525 Cryosphere, 6(4), 881–889, doi:[10.5194/tc-6-881-2012](https://doi.org/10.5194/tc-6-881-2012), 2012.

526 Collins, W. J., Bellouin, N., Doutriaux-Boucher, M., Gedney, N., Halloran, P., Hinton, T., Hughes,
 527 J., Jones, C. D., Joshi, M., Liddicoat, S., Martin, G., O'Connor, F., Rae, J., Senior, C., Sitch, S.,
 528 Totterdell, I., Wiltshire, A. and Woodward, S.: Development and evaluation of an Earth-System
 529 model – HadGEM2, *Geosci. Model Dev.*, 4(4), 1051–1075, doi:[10.5194/gmd-4-1051-2011](https://doi.org/10.5194/gmd-4-1051-2011), 2011.
 530 Comiso, Josephino `Joey`: Bootstrap Sea Ice Concentrations from Nimbus-7 SMMR and DMSP
 531 SSM/I-SSMIS, Version 2, , doi:[10.5067/J6JQLS9EJ5HU](https://doi.org/10.5067/J6JQLS9EJ5HU), 2000.
 532 Donohoe, A. and Battisti, D. S.: The Seasonal Cycle of Atmospheric Heating and Temperature, *J.*
 533 *Climate*, 26(14), 4962–4980, doi:[10.1175/JCLI-D-12-00713.1](https://doi.org/10.1175/JCLI-D-12-00713.1), 2013.
 534 Dufresne, J.-L., Foujols, M.-A., Denvil, S., Caubel, A., Marti, O., Aumont, O., Balkanski, Y.,
 535 Bekki, S., Bellenger, H., Benshila, R., Bony, S., Bopp, L., Braconnot, P., Brockmann, P., Cadule,
 536 P., Cheruy, F., Codron, F., Cozic, A., Cugnet, D., Noblet, N. de, Duvel, J.-P., Ethé, C., Fairhead, L.,
 537 Fichefet, T., Flavoni, S., Friedlingstein, P., Grandpeix, J.-Y., Guez, L., Guilyardi, E., Hauglustaine,
 538 D., Hourdin, F., Idelkadi, A., Ghattas, J., Joussaume, S., Kageyama, M., Krinner, G., Labetoulle, S.,
 539 Lahellec, A., Lefebvre, M.-P., Lefevre, F., Levy, C., Li, Z. X., Lloyd, J., Lott, F., Madec, G.,
 540 Mancip, M., Marchand, M., Masson, S., Meurdesoif, Y., Mignot, J., Musat, I., Parouty, S., Polcher,
 541 J., Rio, C., Schulz, M., Swingedouw, D., Szopa, S., Talandier, C., Terray, P., Viovy, N. and
 542 Vuichard, N.: Climate change projections using the IPSL-CM5 Earth System Model: from CMIP3
 543 to CMIP5, *Clim Dyn*, 40(9–10), 2123–2165, doi:[10.1007/s00382-012-1636-1](https://doi.org/10.1007/s00382-012-1636-1), 2013.
 544 Dussin, R., B. Barnier and L. Brodeau, *The making of Drakkar forcing set DFS5*. Tech. report
 545 DRAKKAR/MyOcean Report 01-04-16, LGGE, Grenoble, France. (2016).
 546 Dwyer, J. G., Biasutti, M. and Sobel, A. H.: Projected Changes in the Seasonal Cycle of Surface
 547 Temperature, *J. Climate*, 25(18), 6359–6374, doi:[10.1175/JCLI-D-11-00741.1](https://doi.org/10.1175/JCLI-D-11-00741.1), 2012.
 548 Fletcher, J. O., The heat budget of the Arctic Basin and its relation to climate, Rep. R-444-PR,
 549 RAND Corp., Santa Monica, Calif., (1965).

550 Gent, P. R., Danabasoglu, G., Donner, L. J., Holland, M. M., Hunke, E. C., Jayne, S. R., Lawrence,
 551 D. M., Neale, R. B., Rasch, P. J., Vertenstein, M., Worley, P. H., Yang, Z.-L. and Zhang, M.: The
 552 Community Climate System Model Version 4, *J. Climate*, 24(19), 4973–4991,
 553 doi:[10.1175/2011JCLI4083.1](https://doi.org/10.1175/2011JCLI4083.1), 2011.

554 Giorgetta Marco A., Jungclaus Johann, Reick Christian H., Legutke Stephanie, Bader Jürgen,
 555 Böttinger Michael, Brovkin Victor, Crueger Traute, Esch Monika, Fieg Kerstin, Glushak Ksenia,
 556 Gayler Veronika, Haak Helmuth, Hollweg Heinz-Dieter, Ilyina Tatiana, Kinne Stefan, Kornblueh
 557 Luis, Matei Daniela, Mauritsen Thorsten, Mikolajewicz Uwe, Mueller Wolfgang, Notz Dirk, Pithan
 558 Felix, Raddatz Thomas, Rast Sebastian, Redler Rene, Roeckner Erich, Schmidt Hauke, Schnur
 559 Reiner, Segschneider Joachim, Six Katharina D., Stockhause Martina, Timmreck Claudia, Wegner
 560 Jörg, Widmann Heinrich, Wieners Karl-H., Claussen Martin, Marotzke Jochem and Stevens Bjorn:
 561 Climate and carbon cycle changes from 1850 to 2100 in MPI-ESM simulations for the Coupled
 562 Model Intercomparison Project phase 5, *Journal of Advances in Modeling Earth Systems*, 5(3),
 563 572–597, doi:[10.1002/jame.20038](https://doi.org/10.1002/jame.20038), 2013.

564 Hezel, P. J., Fichefet, T. and Massonnet, F.: Modeled Arctic sea ice evolution through 2300 in
 565 CMIP5 extended RCPs, *The Cryosphere*, 8(4), 1195–1204, doi:[10.5194/tc-8-1195-2014](https://doi.org/10.5194/tc-8-1195-2014), 2014.

566 Huntington, H. P., Gearheard, S., Holm, L. K., Noongwook, G., Opie, M. and Sanguya, J.: Sea ice
 567 is our beautiful garden: indigenous perspectives on sea ice in the Arctic, in *Sea Ice*, edited by D. N.
 568 Thomas, pp. 583–599, John Wiley & Sons, Ltd., 2017.

569 Johnson, M. and Eicken, H.: Estimating Arctic sea-ice freeze-up and break-up from the satellite
 570 record: A comparison of different approaches in the Chukchi and Beaufort Seas, *Elem Sci Anth*,
 571 4(0), doi:[10.12952/journal.elementa.000124](https://doi.org/10.12952/journal.elementa.000124), 2016.

572 Kröner, N., Kotlarski, S., Fischer, E., Lüthi, D., Zubler, E. and Schär, C.: Separating climate change
 573 signals into thermodynamic, lapse-rate and circulation effects: theory and application to the

574 European summer climate, *Clim Dyn*, 48(9–10), 3425–3440, doi:[10.1007/s00382-016-3276-3](https://doi.org/10.1007/s00382-016-3276-3),
575 2017.

576 Kwok, R. and Rothrock, D. A.: Decline in Arctic sea ice thickness from submarine and ICESat
577 records: 1958–2008, *Geophys. Res. Lett.*, 36(15), L15501, doi:[10.1029/2009GL039035](https://doi.org/10.1029/2009GL039035), 2009.

578 Laidre, K. L., Stern, H., Kovacs, K. M., Lowry, L., Moore, S. E., Regehr, E. V., Ferguson, S. H.,
579 Wiig, Ø., Boveng, P., Angliss, R. P., Born, E. W., Litovka, D., Quakenbush, L., Lydersen, C.,
580 Vongraven, D. and Ugarte, F.: Arctic marine mammal population status, sea ice habitat loss, and
581 conservation recommendations for the 21st century, *Conservation Biology*, 29(3), 724–737,
582 doi:[10.1111/cobi.12474](https://doi.org/10.1111/cobi.12474), 2015.

583 Lindsay, R. and Schweiger, A.: Arctic sea ice thickness loss determined using subsurface, aircraft,
584 and satellite observations, *The Cryosphere*, 9(1), 269–283, doi:[10.5194/tc-9-269-2015](https://doi.org/10.5194/tc-9-269-2015), 2015.

585 Markus, T., Stroeve, J. C. and Miller, J.: Recent changes in Arctic sea ice melt onset, freeze-up, and
586 melt season length, *J. Geophys. Res.*, 114(C12), C12024, doi:[10.1029/2009JC005436](https://doi.org/10.1029/2009JC005436), 2009.

587 Maslanik, J., Stroeve, J., Fowler, C. and Emery, W.: Distribution and trends in Arctic sea ice age
588 through spring 2011, *Geophys. Res. Lett.*, 38(13), L13502, doi:[10.1029/2011GL047735](https://doi.org/10.1029/2011GL047735), 2011.

589 Massonnet, F., Fichefet, T., Goosse, H., Bitz, C. M., Philippon-Berthier, G., Holland, M. M. and
590 Barriat, P.-Y.: Constraining projections of summer Arctic sea ice, *The Cryosphere*, 6(6), 1383–
591 1394, doi:[10.5194/tc-6-1383-2012](https://doi.org/10.5194/tc-6-1383-2012), 2012.

592 Maykut, G. A.: The surface heat and mass balance. In *The Geophysics of Sea Ice*, edited by N.
593 Untersteiner, Plenum Press, New York, 146, 395–463, 1986.

594 Maykut, G. A. and Untersteiner, N.: Some results from a time-dependent thermodynamic model of
595 sea ice, *J. Geophys. Res.*, 76(6), 1550–1575, doi:[10.1029/JC076i006p01550](https://doi.org/10.1029/JC076i006p01550), 1971.

596 Melia, N., Haines, K., Hawkins, E. and Day, J. J.: Towards seasonal Arctic shipping route
597 predictions, *Environ. Res. Lett.*, 12(8), 084005, doi:[10.1088/1748-9326/aa7a60](https://doi.org/10.1088/1748-9326/aa7a60), 2017.

598 Notz, D., Jahn, A., Holland, M., Hunke, E., Massonnet, F., Stroeve, J., Tremblay, B. and
599 Vancoppenolle, M.: The CMIP6 Sea-Ice Model Intercomparison Project (SIMIP): understanding
600 sea ice through climate-model simulations, *Geosci. Model Dev.*, 9(9), 3427–3446,
601 doi:[10.5194/gmd-9-3427-2016](https://doi.org/10.5194/gmd-9-3427-2016), 2016.

602 Notz, D. and Stroeve, J.: Observed Arctic sea-ice loss directly follows anthropogenic CO₂
603 emission, *Science*, aag2345, doi:[10.1126/science.aag2345](https://doi.org/10.1126/science.aag2345), 2016.

604 Parkinson, C. L.: Spatial patterns in the length of the sea ice season in the Southern Ocean, 1979–
605 1986, *J. Geophys. Res.*, 99(C8), 16327–16339, doi:[10.1029/94JC01146](https://doi.org/10.1029/94JC01146), 1994.

606 Parkinson, C. L.: Global Sea Ice Coverage from Satellite Data: Annual Cycle and 35-Yr Trends, *J.*
607 *Climate*, 27(24), 9377–9382, doi:[10.1175/JCLI-D-14-00605.1](https://doi.org/10.1175/JCLI-D-14-00605.1), 2014.

608 Peixoto, J. P. and Oort, A. H.: *Physics of Climate*, 1992 ed., American Institute of Physics, New
609 York., 1992.

610 Perovich, D. K., Grenfell, T. C., Richter-Menge, J. A., Light, B., Tucker, W. B. and Eicken, H.:
611 Thin and thinner: Sea ice mass balance measurements during SHEBA, *Journal of Geophysical*
612 *Research: Oceans*, 108(C3), doi:[10.1029/2001JC001079](https://doi.org/10.1029/2001JC001079), 2003.

613 Perovich, D. K., Light, B., Eicken, H., Jones, K. F., Runciman, K. and Nghiem, S. V.: Increasing
614 solar heating of the Arctic Ocean and adjacent seas, 1979–2005: Attribution and role in the ice-
615 albedo feedback, *Geophys. Res. Lett.*, 34(19), L19505, doi:[10.1029/2007GL031480](https://doi.org/10.1029/2007GL031480), 2007.

616 Persson, P. O. G., Fairall, C. W., Andreas, E. L., Guest, P. S. and Perovich, D. K.: Measurements
617 near the Atmospheric Surface Flux Group tower at SHEBA: Near-surface conditions and surface
618 energy budget, *Journal of Geophysical Research (Oceans)*, 107, 8045, doi:[10.1029/2000JC000705](https://doi.org/10.1029/2000JC000705),
619 2002.

620 Renner, A. H. H., Gerland, S., Haas, C., Spreen, G., Beckers, J. F., Hansen, E., Nicolaus, M. and
 621 Goodwin, H.: Evidence of Arctic sea ice thinning from direct observations, *Geophys. Res. Lett.*,
 622 41(14), 5029–5036, doi:[10.1002/2014GL060369](https://doi.org/10.1002/2014GL060369), 2014.

623 Rotstayn, L. D., Jeffrey, S. J., Collier, M. A., Dravitzki, S. M., Hirst, A. C., Syktus, J. I. and Wong,
 624 K. K.: Aerosol- and greenhouse gas-induced changes in summer rainfall and circulation in the
 625 Australasian region: a study using single-forcing climate simulations, *Atmos. Chem. Phys.*, 12(14),
 626 6377–6404, doi:[10.5194/acp-12-6377-2012](https://doi.org/10.5194/acp-12-6377-2012), 2012.

627 Rousset, C., Vancoppenolle, M., Madec, G., Fichefet, T., Flavoni, S., Barthélemy, A., Benshila, R.,
 628 Chanut, J., Levy, C., Masson, S. and Vivier, F.: The Louvain-La-Neuve sea ice model LIM3.6:
 629 global and regional capabilities, *Geosci. Model Dev.*, 8(10), 2991–3005, doi:[10.5194/gmd-8-2991-](https://doi.org/10.5194/gmd-8-2991-2015)
 630 [2015](https://doi.org/10.5194/gmd-8-2991-2015), 2015.

631 Schmidt, G. A., Kelley, M., Nazarenko, L., Ruedy, R., Russell, G. L., Aleinov, I., Bauer, M., Bauer,
 632 S. E., Bhat, M. K., Bleck, R., Canuto, V., Chen, Y.-H., Cheng, Y., Clune, T. L., Del Genio, A., de
 633 Fainchtein, R., Faluvegi, G., Hansen, J. E., Healy, R. J., Kiang, N. Y., Koch, D., Lacis, A. A.,
 634 LeGrande, A. N., Lerner, J., Lo, K. K., Matthews, E. E., Menon, S., Miller, R. L., Oinas, V., Olosa,
 635 A. O., Perlwitz, J. P., Puma, M. J., Putman, W. M., Rind, D., Romanou, A., Sato, M., Shindell, D.
 636 T., Sun, S., Syed, R. A., Tausnev, N., Tsigaridis, K., Unger, N., Voulgarakis, A., Yao, M.-S. and
 637 Zhang, J.: Configuration and assessment of the GISS ModelE2 contributions to the CMIP5 archive,
 638 *J. Adv. Model. Earth Syst.*, 6(1), 141–184, doi:[10.1002/2013MS000265](https://doi.org/10.1002/2013MS000265), 2014.

639 Semtner, A. J.: A Model for the Thermodynamic Growth of Sea Ice in Numerical Investigations of
 640 Climate, *J. Phys. Oceanogr.*, 6(3), 379–389, doi:[10.1175/1520-](https://doi.org/10.1175/1520-0485(1976)006<0379:AMFTTG>2.0.CO;2)
 641 [0485\(1976\)006<0379:AMFTTG>2.0.CO;2](https://doi.org/10.1175/1520-0485(1976)006<0379:AMFTTG>2.0.CO;2), 1976.

642 Serreze, M. C., Crawford, A. D., Stroeve, J. C., Barrett, A. P. and Woodgate, R. A.: Variability,
 643 trends, and predictability of seasonal sea ice retreat and advance in the Chukchi Sea, *J. Geophys.*
 644 *Res. Oceans*, 121(10), 7308–7325, doi:[10.1002/2016JC011977](https://doi.org/10.1002/2016JC011977), 2016.

645 Shepherd, T. G.: Atmospheric circulation as a source of uncertainty in climate change projections,
646 Nature Geoscience, 7(10), 703–708, doi:[10.1038/ngeo2253](https://doi.org/10.1038/ngeo2253), 2014.

647 Smith, L. C. and Stephenson, S. R.: New Trans-Arctic shipping routes navigable by midcentury,
648 PNAS, 110(13), E1191–E1195, doi:[10.1073/pnas.1214212110](https://doi.org/10.1073/pnas.1214212110), 2013.

649 Stammerjohn, S., Massom, R., Rind, D. and Martinson, D.: Regions of rapid sea ice change: An
650 inter-hemispheric seasonal comparison, Geophys. Res. Lett., 39(6), L06501,
651 doi:[10.1029/2012GL050874](https://doi.org/10.1029/2012GL050874), 2012.

652 Steele, M., Ermold, W. and Zhang, J.: Arctic Ocean surface warming trends over the past 100 years,
653 Geophys. Res. Lett., 35(2), L02614, doi:[10.1029/2007GL031651](https://doi.org/10.1029/2007GL031651), 2008.

654 Steele, M. and Dickinson, S.: The phenology of Arctic Ocean surface warming, J. Geophys. Res.
655 Oceans, 121(9), 6847–6861, doi:[10.1002/2016JC012089](https://doi.org/10.1002/2016JC012089), 2016.

656 Steiner, N. S., Christian, J. R., Six, K. D., Yamamoto, A. and Yamamoto-Kawai, M.: Future ocean
657 acidification in the Canada Basin and surrounding Arctic Ocean from CMIP5 earth system models,
658 J. Geophys. Res. Oceans, 119(1), 332–347, doi:[10.1002/2013JC009069](https://doi.org/10.1002/2013JC009069), 2014.

659 Stern, H. L. and Laidre, K. L.: Sea-ice indicators of polar bear habitat, The Cryosphere, 10(5),
660 2027–2041, doi:[10.5194/tc-10-2027-2016](https://doi.org/10.5194/tc-10-2027-2016), 2016.

661 Stroeve, J. C., Kattsov, V., Barrett, A., Serreze, M., Pavlova, T., Holland, M. and Meier, W. N.:
662 Trends in Arctic sea ice extent from CMIP5, CMIP3 and observations, Geophys. Res. Lett., 39(16),
663 L16502, doi:[10.1029/2012GL052676](https://doi.org/10.1029/2012GL052676), 2012.

664 Stroeve, J. C., Markus, T., Boisvert, L., Miller, J. and Barrett, A.: Changes in Arctic melt season
665 and implications for sea ice loss, Geophysical Research Letters, 41(4), 1216–1225,
666 doi:[10.1002/2013GL058951](https://doi.org/10.1002/2013GL058951), 2014.

667 Stroeve, J. C., Crawford, A. D. and Stammerjohn, S.: Using timing of ice retreat to predict timing of
668 fall freeze-up in the Arctic, *Geophys. Res. Lett.*, 43(12), 2016GL069314,
669 doi:[10.1002/2016GL069314](https://doi.org/10.1002/2016GL069314), 2016.

670 Thomson, D. J.: The seasons, global temperature, and precession, *Science*, 268(5207), 59–68,
671 doi:[10.1126/science.268.5207.59](https://doi.org/10.1126/science.268.5207.59), 1995.

672 Uotila, P., Iovino, D., Vancoppenolle, M., Lensu, M. and Rousset, C.: Comparing sea ice,
673 hydrography and circulation between NEMO3.6 LIM3 and LIM2, *Geosci. Model Dev.*, 10(2),
674 1009–1031, doi:[10.5194/gmd-10-1009-2017](https://doi.org/10.5194/gmd-10-1009-2017), 2017.

675 Vancoppenolle, M., Bopp, L., Madec, G., Dunne, J., Ilyina, T., Halloran, P. R. and Steiner, N.:
676 Future Arctic Ocean primary productivity from CMIP5 simulations: Uncertain outcome, but
677 consistent mechanisms, *Global Biogeochem. Cycles*, 27(3), 605–619, doi:[10.1002/gbc.20055](https://doi.org/10.1002/gbc.20055),
678 2013.

679 Voldoire, A., Sanchez-Gomez, E., Méliá, D. S. y, Decharme, B., Cassou, C., Sénési, S., Valcke, S.,
680 Beau, I., Alias, A., Chevallier, M., Déqué, M., Deshayes, J., Douville, H., Fernandez, E., Madec,
681 G., Maisonnave, E., Moine, M.-P., Planton, S., Saint-Martin, D., Szopa, S., Tyteca, S., Alkama, R.,
682 Belamari, S., Braun, A., Coquart, L. and Chauvin, F.: The CNRM-CM5.1 global climate model:
683 description and basic evaluation, *Clim Dyn*, 40(9–10), 2091–2121, doi:[10.1007/s00382-011-1259-](https://doi.org/10.1007/s00382-011-1259-y)
684 [y](https://doi.org/10.1007/s00382-011-1259-y), 2013.

685 Wang, M. and Overland, J. E.: Projected future duration of the sea-ice-free season in the Alaskan
686 Arctic, *Progress in Oceanography*, 136, 50–59, doi:[10.1016/j.pocean.2015.01.001](https://doi.org/10.1016/j.pocean.2015.01.001), 2015.

687 Wassmann, P. and Reigstad, M.: Future Arctic Ocean Seasonal Ice Zones and Implications for
688 Pelagic-Benthic Coupling, *Oceanography*, 24(3), 220–231, doi:[10.5670/oceanog.2011.74](https://doi.org/10.5670/oceanog.2011.74), 2011.

689 Wu, T., Song, L., Li, W., Wang, Z., Zhang, H., Xin, X., Zhang, Y., Zhang, L., Li, J., Wu, F., Liu,
690 Y., Zhang, F., Shi, X., Chu, M., Zhang, J., Fang, Y., Wang, F., Lu, Y., Liu, X., Wei, M., Liu, Q.,

691 Zhou, W., Dong, M., Zhao, Q., Ji, J., Li, L. and Zhou, M.: An overview of BCC climate system
692 model development and application for climate change studies, *Acta Meteorol Sin*, 28(1), 34–56,
693 doi:[10.1007/s13351-014-3041-7](https://doi.org/10.1007/s13351-014-3041-7), 2014.

694 Yu, L., X. Jin, and R. A. Weller, Multidecade Global Flux Datasets from the Objectively Analyzed
695 Air-sea Fluxes (OAFlux) Project: Latent and sensible heat fluxes, ocean evaporation, and related
696 surface meteorological variables. Tech. Report Woods Hole Oceanographic Institution, OAFlux
697 Project Technical Report. OA-2008-01, 64pp. Woods Hole. Massachusetts (2008).

Tables and Figures

Table 1. Linear trends in ice retreat and advance dates over 2000-2200 (200 years), and long-term ice advance amplification ratios for the individual and mean CMIP5 models and for the 1D model. Trends and ratios are given as median \pm interquartile range over the seasonal ice zone where trends are significant at a 95% confidence level ($p = 0.05$).

	r_r (days / decade)	r_a (days / decade)	$R_{a/r}^{long}$	Reference
CCSM4	-6.6 ± 2.1	13.4 ± 7.3	2.0 ± 0.6	<i>Gent et al., 2011</i>
CNRM-CM5	-8.0 ± 2.8	13.5 ± 5.9	1.7 ± 0.3	<i>Voldoire et al., 2013</i>
CSIRO-Mk3-6-0	-6.1 ± 3.3	10.4 ± 4.0	1.7 ± 0.6	<i>Rotstayn et al., 2012</i>
GISS-E2-H	-2.8 ± 0.6	5.1 ± 1.6	1.8 ± 0.4	<i>Schmidt et al., 2014</i>
MPI-ESM-LR	-8.6 ± 2.8	15.2 ± 8.1	1.8 ± 0.4	<i>Giorgetta et al., 2013</i>
bcc-csm1-1	-5.2 ± 1.3	9.7 ± 2.6	1.9 ± 0.4	<i>Wu et al., 2014</i>
GISS-E2-R	-2.0 ± 0.4	3.4 ± 0.8	1.8 ± 0.3	<i>Schmidt et al., 2014</i>
HadGEM2-ES	-9.1 ± 3.0	18.6 ± 7.6	1.9 ± 0.5	<i>Collins et al., 2011</i>
IPSL-CM5A-LR	-5.7 ± 1.2	11.1 ± 3.8	1.9 ± 0.5	<i>Dufresne et al., 2013</i>
MEAN CMIP5	-6.0 ± 2.0	11.1 ± 4.6	1.8 ± 0.4	
1D model	$-3.1 \pm \text{n.a.}$	$6.0 \pm \text{n.a.}$	$1.9 \pm \text{n.a.}$	

Figure 1. Evolution of the ice seasonality diagnostics (ice retreat date, blue; and ice advance date, orange): (a) CMIP5 median and interquartile range, with corresponding range of satellite derived-values (green rectangles 1980-2015) over the 70-80°N latitude band; (b) one-dimensional ice-ocean model results. The ice-free period (L_w), the photoperiod (L_p) and the average polar night (gray rectangle) are also depicted. Note that the systematic difference between observations and CMIP5 models is reduced when accounting for the systematic bias due to the daily interpolation of monthly means in CMIP5 models (See Methods and Tab. S2).

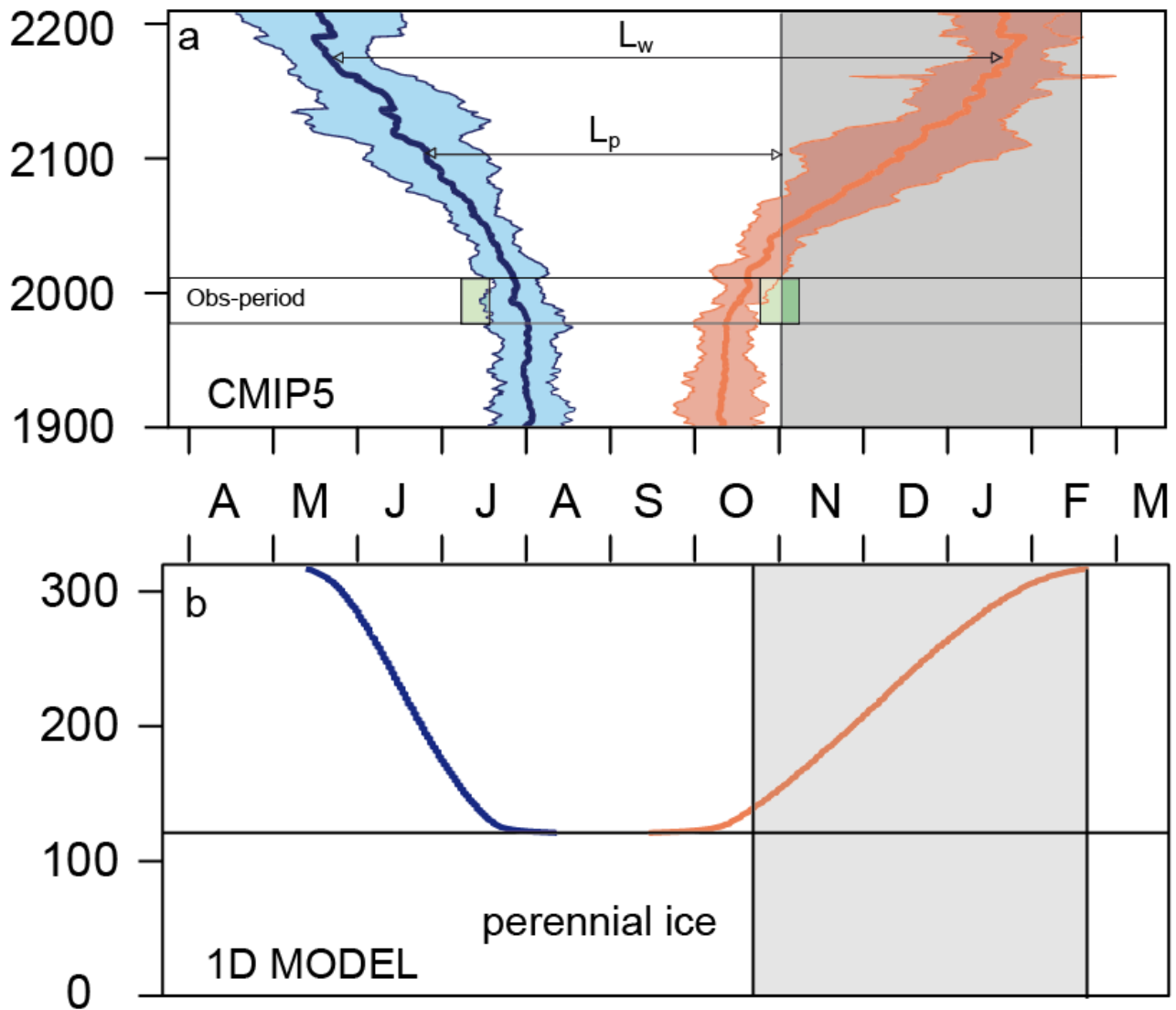


Figure 2. Maps and frequency histograms of (a,d) ice retreat date (b,e) ice advance date and (c,f) ice-free season length over 1980-2015 (36 years), based on (a,b,c) passive microwave satellite concentration retrievals (Comiso, 2000; updated 2015) and (d,e,f) daily concentration fields averaged over CMIP5 models. Median \pm IQR refers to all points in the seasonal ice zone. See figure S3 for individual models.

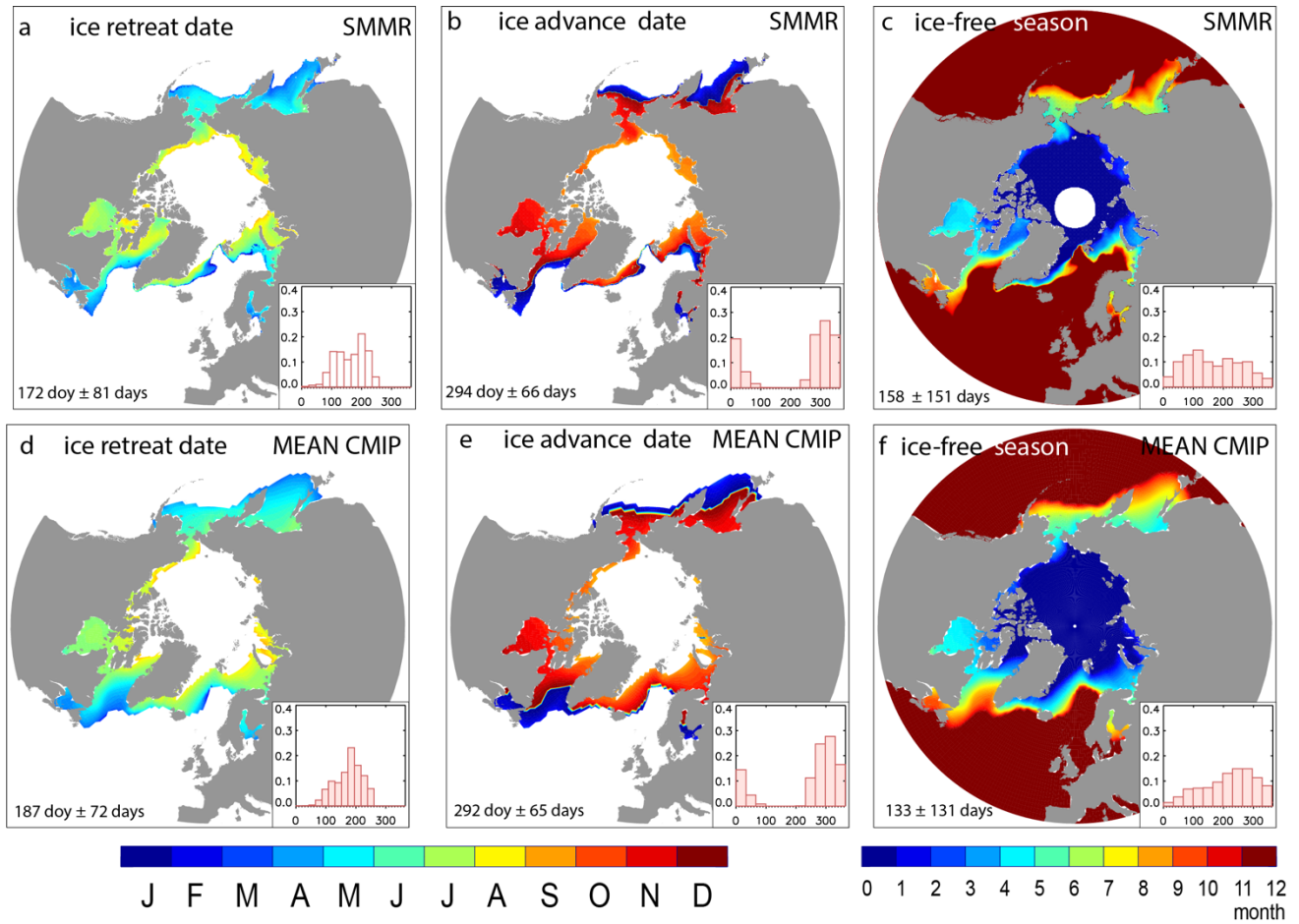


Figure 3. Maps and frequency histograms of linear trends (for hatched zones only) in (a,d) ice retreat date (b,e,) ice advance date and (c,f) ice-free season length-over 1980-2015 (36 years), based on (a,b,c) passive microwave satellite concentration retrievals (Comiso, 2000; updated 2015); (d,e,f) the mean CMIP5 models. Hatching refers to the 95% confidence interval ($p=0.05$). Median \pm IQR refers to significant pixels with at least 1/3 of the years with defined retreat and ice advance dates. See figure S4 for individual models.

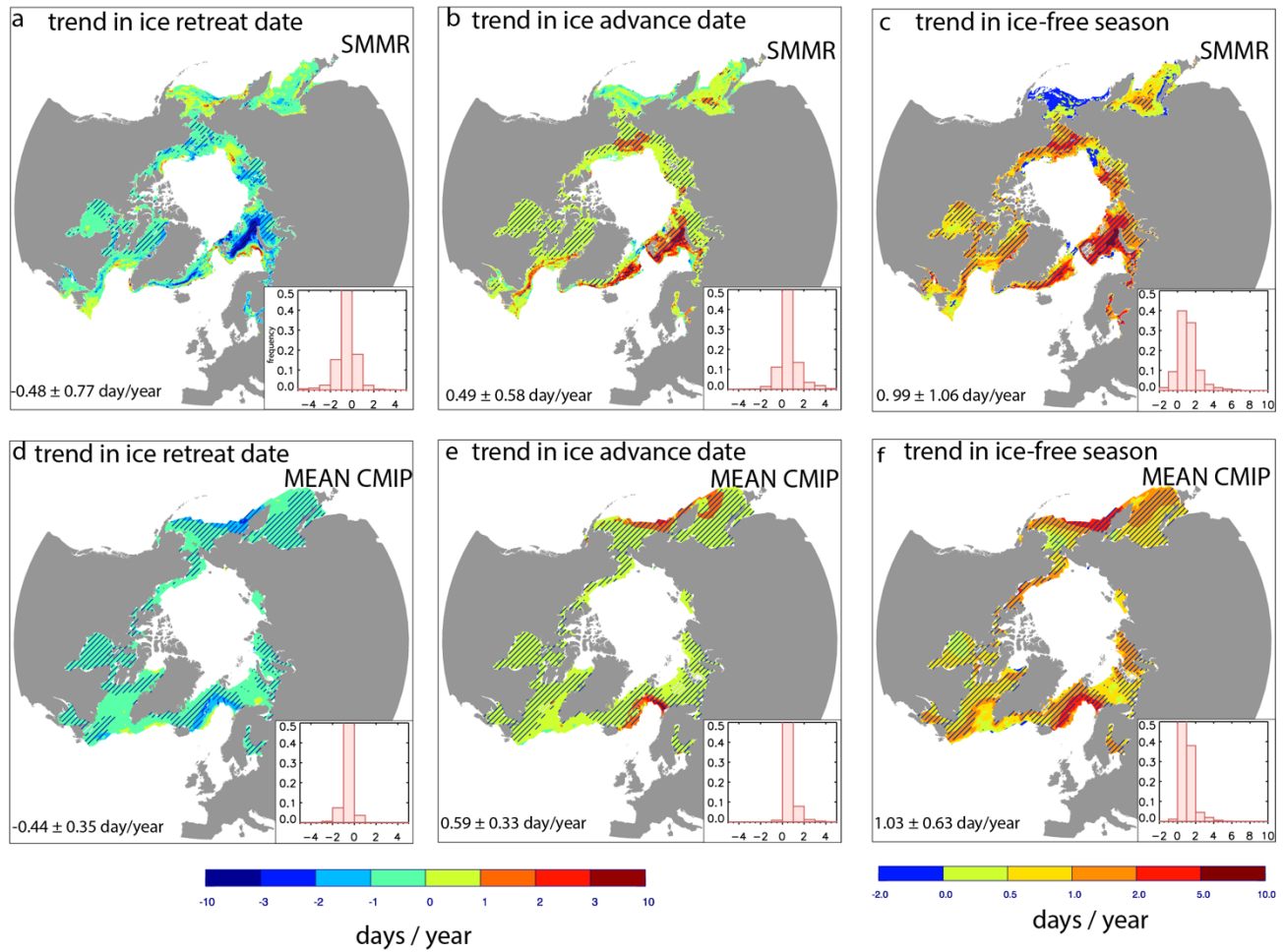


Figure 4. Long-term ice advance vs. retreat amplification coefficient from passive microwave ice concentration retrievals (SMMR; over 1980-2015); and for all individual models over 1980-2015, 2015-2050 and 2050-2085. We use a 75% ($p=0,25$) confidence interval for this specific computation. The same figures for $p = 0.05$ are available as Supplementary Material (Fig. S9).

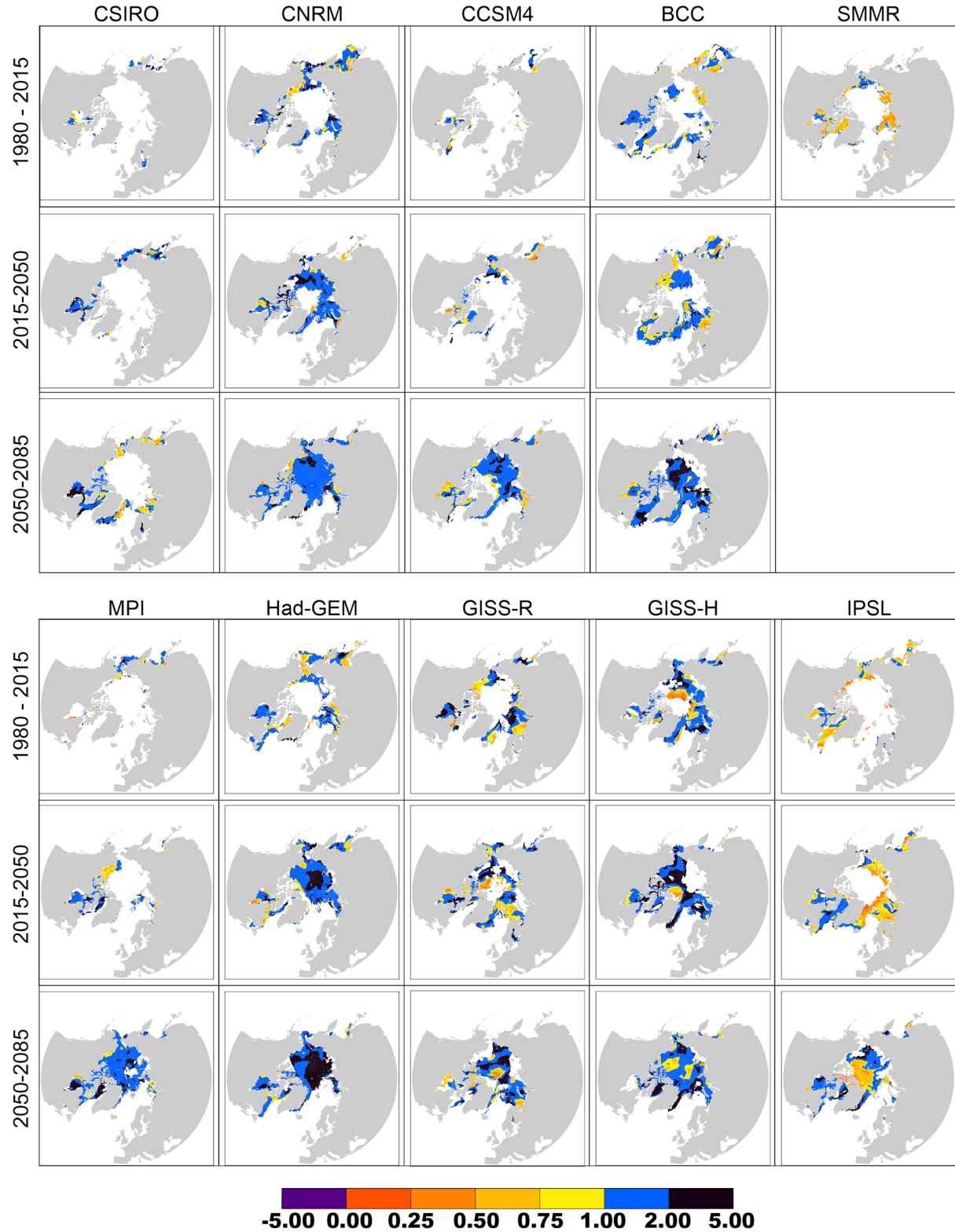


Figure 5. Short-term ice advance vs. retreat amplification coefficient from passive microwave ice concentration retrievals (SMMR; over 1980-2015); and for all individual models over 1980-2015, 2015-2050, 2050-2085.

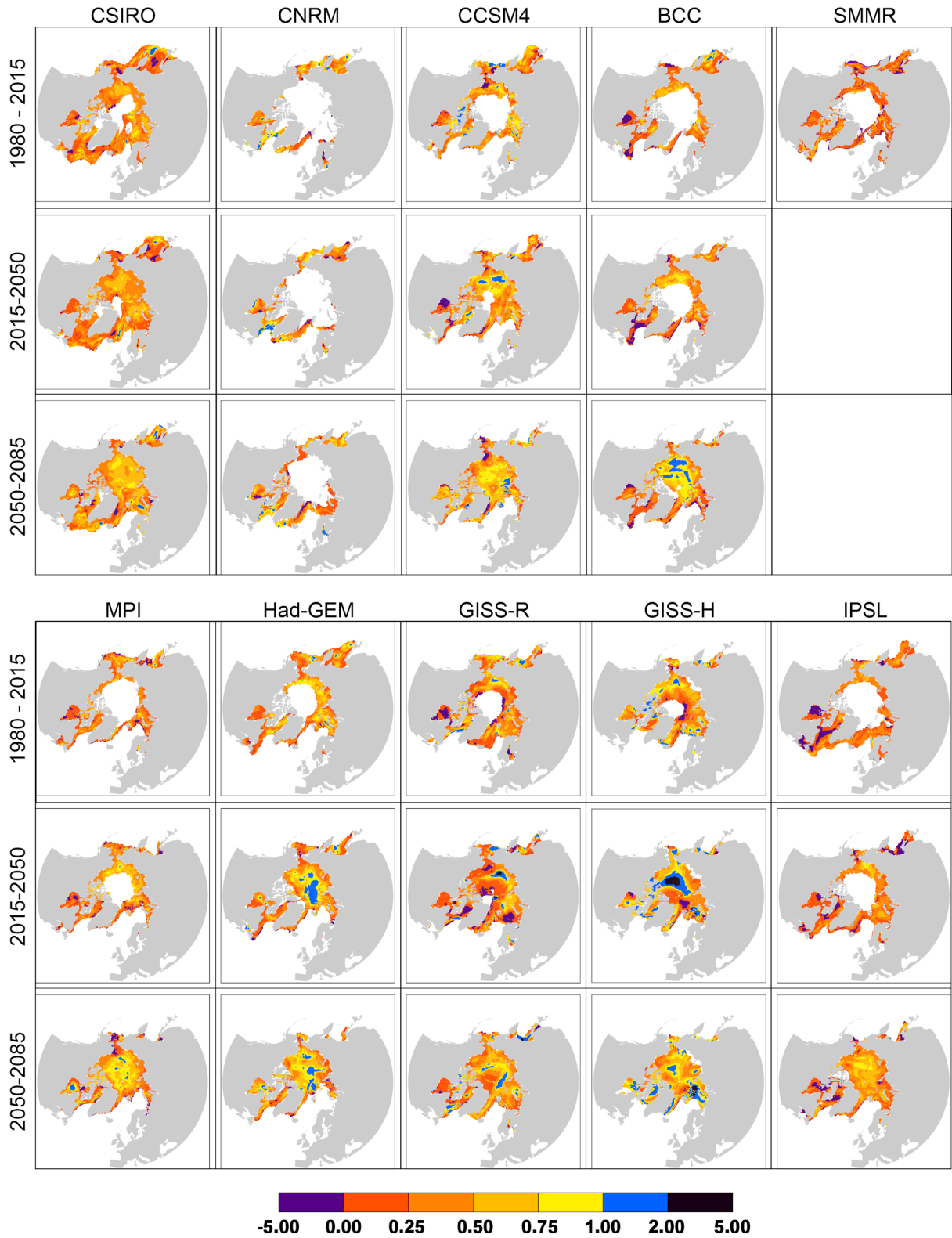


Figure 6. (Top) Energetics of ice retreat and advance in the simple model: net atmospheric (solid) and solar (yellow) heat fluxes to the ocean; SST (dash), depicted for years 150 and 210. **(Bottom)** Annual evolution of the simulated sea surface temperature, averaged over the seasonal ice zone, for two decades of reference (2015-2025, 2075-2085) as simulated by the IPSL_CM5A_LR model and showing the same temporal asymmetry as in the simple model.

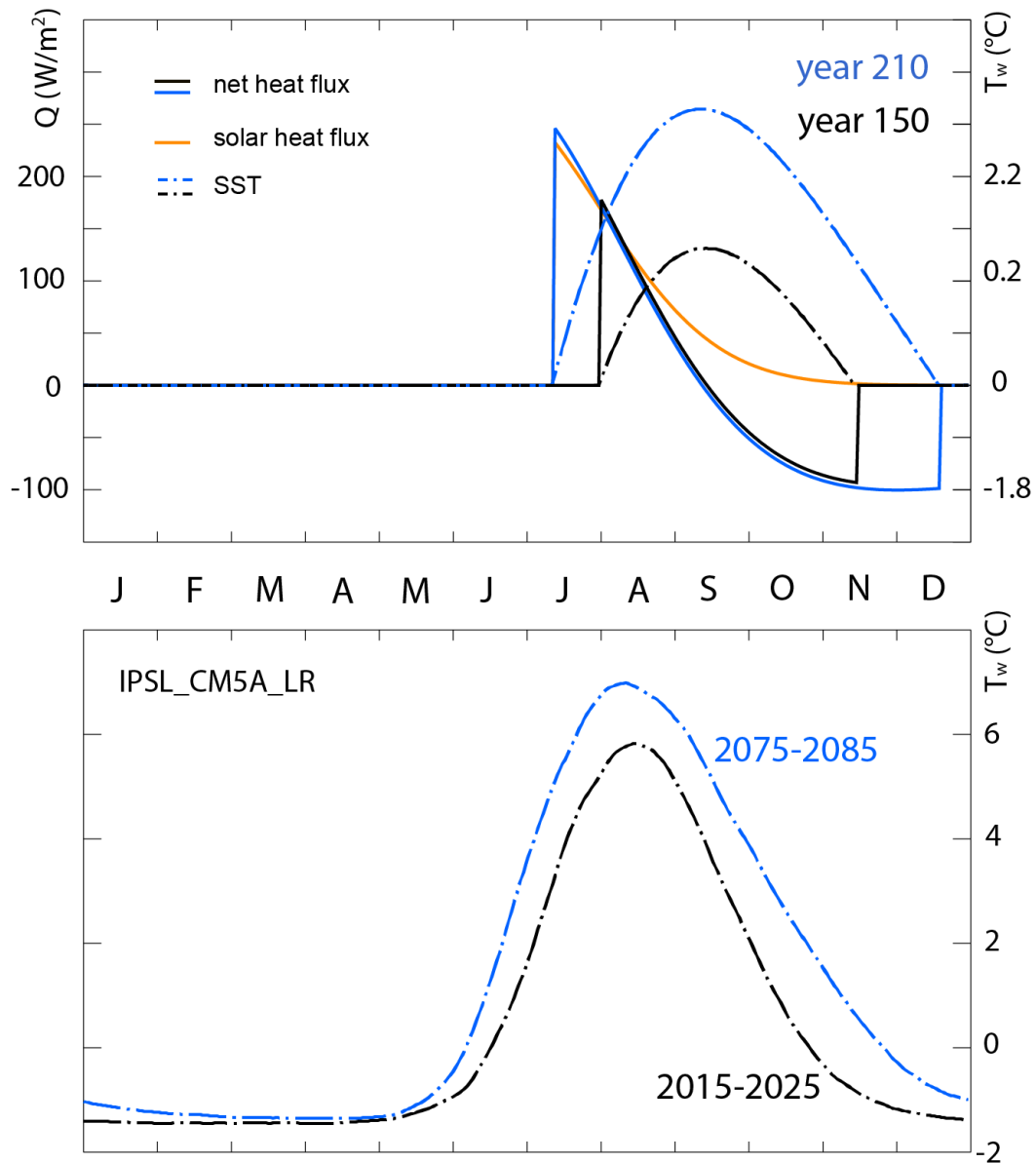


Figure A1. Correspondence between the long-term ice advance vs. retreat amplification coefficient $R_{a/r}^{long}$ and the ice-free ocean energy budget, based on the 1D model. Red circles: direct diagnostic $\Delta d_a / \Delta d_r$ derived from annual time series of d_r and d_a . Orange line: water energetics-derived diagnostic, exact solution, i.e. (10) divided by Δd_a . Blue line: simplified water energetics-derived diagnostic, i.e. (11) divided by Δd_r .

